Middle–late Holocene Caribbean aridity inferred from foraminifera and elemental data in sediment cores from two Cuban lagoons

Braden R.B. Gregory [a,*], Matthew Peros [b], Eduard G. Reinhardt [a], Jeffrey P. Donnelly [c]

[a] School of Geography and Earth Sciences, McMaster University, 1280 Main Street West, Hamilton, Ontario L8S 4M1, Canada
[b] Department of Environmental Studies and Geography, Bishop's University, 2600 College Street, Sherbrooke, Quebec J1M 1Z7, Canada
[c] Coastal Systems Group, Woods Hole Oceanographic Institution, 86 Water Street, Woods Hole, MA 02543, United States

ARTICLE INFO

ABSTRACT

Coastal lagoons are rarely used as paleoclimate archives because of their complex geomorphic histories, which can be affected by both climate and sea-level change. Combined foraminiferal and XRF element analysis of sediment cores from Punta de Cartas and Playa Bailen, Cuba, isolated the effects of climate change (wet vs dry) on the lagoon environments. Foraminiferal assemblages from both Punta de Cartas and Playa Bailen show increasing diversity over the past 4000 yr BP, with a prominent increase at ~1400–1100 yr BP. Assemblages were initially dominated by *Ammonia* spp. (e.g., *Ammonia tepida*) and *Elphidium* spp. (e.g., *Elphidium excavatum*), indicating brackish conditions, but increased miliolid species (e.g., *Triloculina* spp. *Quinqueloculina* spp.), indicate a shift to more marine conditions up-core. Correspondingly, terrigenous input to the lagoon (Fe, Ti, Ti/Ca and K) declined over the past 4000 yr BP with a flexion at ~1200–1100 yr BP that is likely a consequence of decreasing precipitation. Fe, Ti and K have been used as proxies for detrital erosion and transport rates in tropical and subtropical basins, with greater input during wet periods, but have rarely been applied to shallow lagoon systems. Coincident changes in the XRF and foraminiferal data indicate decreased freshwater input to the lagoon and support an inference for the onset of drier climate conditions. Similar temporal patterns in the foraminifera and XRF records from the two lagoons, which are ~10 km apart, suggest a regional climate influence, with increasingly arid conditions developing since the middle-Holocene (4 kyr BP). A pronounced drying over the last ~1200 years agrees with other climate records from the Caribbean.

1. Introduction

The Caribbean supplies moisture for much of North America. Subtle changes in sea surface temperature and atmospheric circulation in the circum-Caribbean influences the climate of the surrounding region (Haug et al., 2001; Wang et al., 2006). Reconstructions of Caribbean climate during the Holocene are a basis for understanding these teleconnections, and better predicting future global climate. Previous paleoclimate studies in the Caribbean focused on archives in the Dominican Republic (Donnelly and Woodruff, 2007; Woodruff et al., 2008; Lane et al., 2011, 2014), Belize (Gischler and Storz, 2009; McCloskey and Keller, 2009; Wooller et al., 2009), Jamaica (Holmes et al., 1995), Haiti (Hodell et al, 1991; Higuera-Gundy et al., 1999), Venezuela (Haug et al., 2001, 2003; Wurtzel et al., 2013), Puerto Rico (Lane et al., 2013), St Martin (Malaizé et al., 2011), Grenada (Fritz et al., 2011) and the Yucatan Peninsula (Medina-Elizalde et al., 2010; Frappier et al., 2014). Paleoclimate information from Cuba, however, is

limited to speleothem δ¹⁸O records (Fensterer et al., 2013) and palynological, microfossil and isotope work from a lagoon sediment core (Peros et al., 2007a,b). More temporal and spatial data are needed to constrain Caribbean climate change, but there are few lakes that provide suitable archives. Although speleothem records are an excellent data source, a breadth of proxies are needed to provide a comprehensive understanding of climate forcing, and are vital for testing climate models and examining the importance of climate feedbacks (Sloan and Barron, 1992; Masson-Delmotte et al., 2005; Braconnot et al., 2012). A recent analysis by the Paleoclimate Modeling Intercomparison Project showed relatively poor agreement between modeled and observed tropical sea surface temperatures, emphasizing the importance of climate feedbacks in tropical regions, and requiring further investigation using proxy data (Braconnot et al., 2012).

Coastal environments, such as estuaries and lagoons, are not often used for reconstructing paleoclimate trends because of uncertainties regarding their geomorphic evolution (e.g., barrier formation, sea-level change, etc.,). Foraminifera and ostracods have been used extensively for reconstructing paleoenvironmental evolution of estuaries and lagoons, as the organisms respond predictably to salinity change. Within a given lagoon or estuary, salinity is a function of sea-level, barrier configuration and freshwater input, the latter a consequence of changing

precipitation and evaporation rates. The multiple variables influencing salinity can make identification of the primary cause of salinity shifts difficult (Brewster-Wingard and Ishman, 1999; Cann et al., 2000; Cann and Cronin, 2004; Peros et al., 2007a; Gabriel et al., 2008; van Hengstum et al., 2010; Cheng et al., 2012).

Trace element analysis of sediments has become more common with the development of high-resolution X-ray fluorescence (XRF) core scanning in the early 2000s, which enables rapid measurement of trace element composition in sediment (Haug et al., 2001; Lamy et al., 2001; Rothwell, 2006). The trace element composition reflects a combination of deposited mineral material, solutes in the water scavenged by organic flocculants and clays, and biotic and abiotic precipitates from the water column (e.g., calcareous and siliceous shells and tests), all of which can be affected by early diagenesis in the uppermost sediment (Engstrom and Wright, 1984; Battistion et al., 2003). Different mineral combinations have been used to identify a wide range of factors that affect depositional processes specific to environments or basins (Rothwell et al., 2006; Thanachit et al., 2006; Thomson et al., 2006). Fe, Ti, Ti/Ca and K have been used to indicate erosion and transport of continental rocks and alluvium within drainage basins (Haug et al., 2001; Thanachit et al., 2006). Increased precipitation can intensify transport of terrigenous elements towards the basin depocenter via runoff (e.g., Haug et al., 2001; Lamy et al., 2001). The relationship between precipitation and terrigenous sediment input has been established in many environments, including deep ocean basins (Yarincik et al., 2000; Haug et al., 2001; Mora and Martinez, 2005; Yao

et al., 2012), continental shelves and slopes (Arz et al., 1998; Lamy et al., 2001; Zabel et al., 2001; Bertrand et al., 2007; Mahiques et al., 2009) and lakes (Haberzettl et al., 2008; Sáez et al., 2009; Warrier and Shankar, 2009; Löwemark et al., 2011). Similar relationships should apply to lagoons if they are closed or semi-closed relative to the larger basin, but this has not been investigated.

Here we present high-resolution XRF and foraminiferal data from sediment cores taken in two Cuban lagoons, Punta de Cartas and Playa Bailen. The foraminiferal data document salinity shifts over the past ~4000 years, whereas the trace elements (Fe, Ti, Ti/Ca and K) reflect changes in the magnitude of erosion, which is influenced by rainfall. Comparison of the two datasets from two separate lagoons enabled isolation of precipitation and its influence on salinity, indicating a regional climate response.

2. Study area

We analyzed sediment cores from two lagoons on the southwest coast of Cuba (Fig. 1). Punta de Cartas is an elliptical, restricted lagoon on the north shore of the Bahia de Cortez. Punta de Cartas is the seaward segment of a larger wetland system that is composed of dense red mangrove forests (*Rhizophora mangle*) and shallow ponds (Fig. 1C). A ~100-m barrier of developing mangrove, beach grasses and sand separates the lagoon from the ocean. Presently, a 200-m-long, 5-m-wide channel intersects this barrier, connecting the lagoon to the ocean.
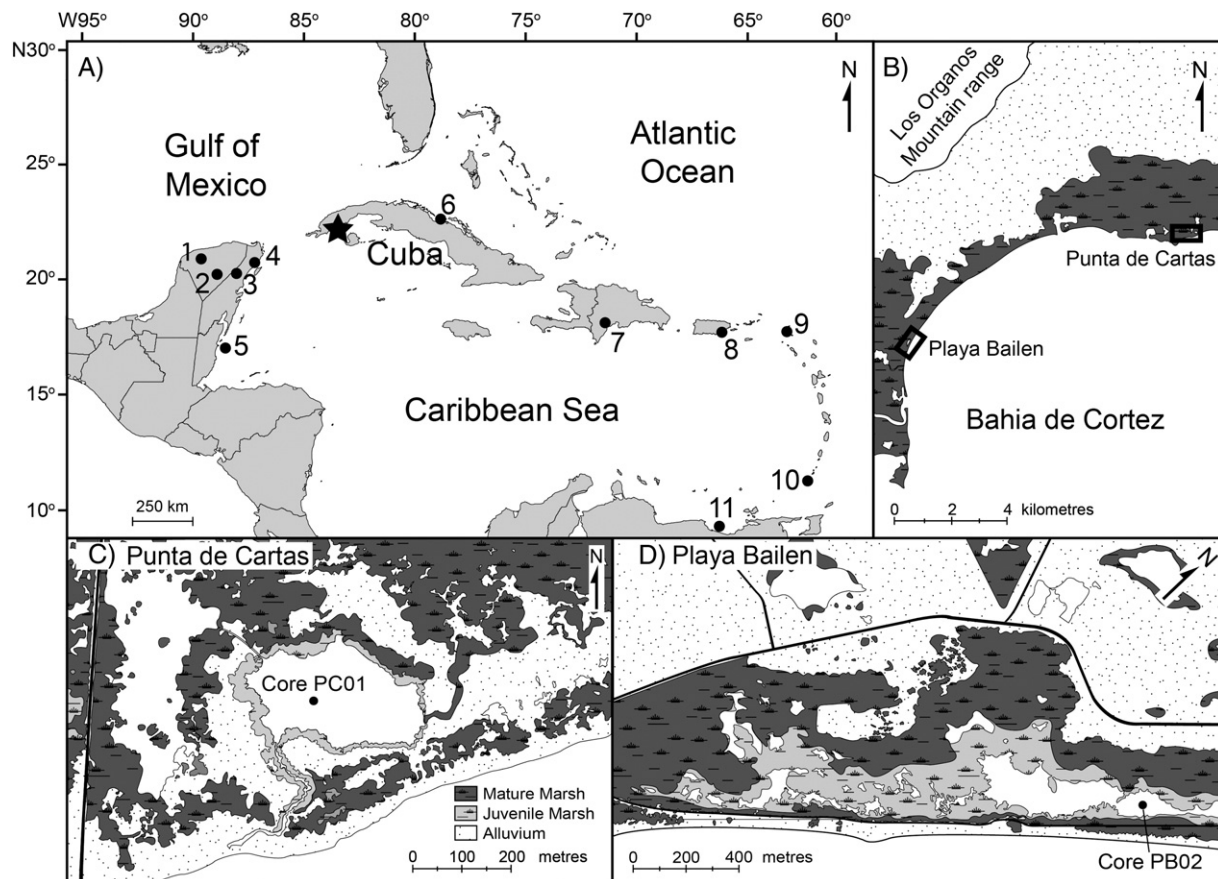
Fig. 1. Map of the study area. (1A) The location of the study areas, demarcated by the black star, and other climate records from the circum-Caribbean. Other locations include (1) Aquada X'caamal, Mexico (Hodell et al., 2005); (2) Lake Chichancanab, Mexico (Hodell et al., 1995); (3) Lake Punta Laguna, Mexico (Curtis et al., 1996); (4) Puerto Morelos, Mexico (Islebe and Sanchez, 2002); (5) Turneffe Atoll, Belize (Wooller et al., 2009); (6) Laguna de la Leche, Cuba (Peros et al., 2007a,b); (7) Laguna Castilla, Dominican Republic (Lane et al., 2009, 2014); (8) Laguna Playa Grande, Puerto Rico (Donnelly and Woodruff, 2007; Woodruff et al., 2008); (9) Grand Case Pond, St Martin (Malaizé et al., 2011); (10) Lake Antoine, Grenada (Fritz et al., 2011); and (11) the Cariaco Basin, Venezuela (Haug et al., 2001). (1B) Aerial view of the area surrounding Punta de Cartas and Playa Bailen showing their relation to the Los Organos mountain range to the north, and the Bahia de Cortez to the south. (1C) The first of two study sites, Punta de Cartas, and the location of core PC01 (black circle). (1D) Playa Bailen, the second study site, with the location of core PB02 (black circle).

Playa Bailen is located on the western shore of the Bahia de Cortez, 15 km southwest of Punta de Cartas. Unlike Punta de Cartas, Playa Bailen is topographically isolated from the surrounding wetlands to the north and west (Fig. 1D). Playa Bailen is elongated parallel to the shoreline (NE–SW) and is separated from the ocean by a ~100-m barrier. Presently, this barrier supports a small community and public beach, which has altered its natural condition. Swaths of red mangrove fringe Playa Bailen and extend into the lagoon, and there are small stands of mangrove in the open-water areas.

Punta de Cartas and Playa Bailen are on the sheltered shore of Bahia de Cortez, the westernmost extent of Cuba's continental shelf, which extends 15 km offshore at this location. The area north of the lagoons is a shallow coastal plain, 10–15 km wide, comprised of alluvium from the southern terranes of the Los Organos mountain range further to the north (Iturralde-Vinent, 1994; Fig. 1B). The mountainous terranes are composed of Lower Jurassic siliciclastic, coastal, and shallow marine sediments overlain by Oxfordian shallow-water conglomerates and carbonate platform sequences; intercalations of tholeiitic basalt occur throughout these sequences (Iturralde-Vinent, 1994).

The Pinar del Rio province has an average temperature between 24 and 26 °C, with a summer wet season from May to October, and a dry season during the winter from November to April (Oliva et al., 1989). The southern coast of Pinar del Rio receives 1200–1400 mm of rainfall a year, ~1000 mm of which falls during the wet season. The wet season precipitation is distinctly bimodal, with maxima in June and August (Seifriz, 1943; Oliva et al., 1989).

3. Methods

Sediment cores were collected from Punta de Cartas (22°10′23.46″N, 83°49′35.80″W; Fig. 1C) and Playa Bailen (22°08′22.83″N, 83°57′31.18″W; Fig. 1D) using a tube fitted with a piston for the upper 25 cm of sediment, and a Russian peat corer for sediments below 25 cm (Fig. 1). Water depth at both coring sites was ~70 cm at the time of sampling. Core PC01 was 275 cm long and core PB02 was 330 cm long. Grey basal clay prevented further penetration at both locations.

Cores were analyzed for elemental composition using a Cox ITRAX core scanner at the Woods Hole Oceanographic Institution. Counts for 25 elements were recorded at 1-mm intervals for 20 s using a Mo X-ray source. High-resolution radiographic (XRI) and photographic (RGB) images of PC01 and PB02 were also obtained during analysis, and used to document sediment structures and organic content.

Organic matter (OM), silicate and carbonate content (CaCO$_3$) throughout the core were determined using loss on ignition (LOI) analysis following procedures outlined by Dean (1974) and Heiri et al. (2001). Approximately 3 cm^3 of sediment was sampled at 1-cm intervals, weighed and dried overnight at 110 °C. Once dry, samples were weighed and heated in a muffle furnace at 550 °C for 4 h, allowed to cool in a desiccator, then re-weighed to provide estimates of organic matter (OM) content. Samples were then heated to 1000 °C for two hours to remove carbonates. CaCO$_3$ was calculated using the difference in weight between combustion steps divided by 0.44, which accounts for the proportion of CO$_2$ in CaCO$_3$ (Dean, 1974).

Foraminifera in cores PC01 and PB02 were examined at 10-cm intervals. Approximately 5 cm^3 of sediment was disaggregated and wet-sieved at 63 μm to isolate foraminifera. Dry sediment was split and examined using a binocular dissecting microscope (90× maximum magnification) and foraminiferal identification followed that of Poag (1981) and Javaux and Scott (2003). Generally, 200 foraminifera were counted per sample to ensure statistical significance (Patterson and Fishbein, 1989; Fatela and Taborda, 2002). Only a few dominant species, however, were used as indicators of environmental change, as their abundance clearly showed salinity trends. Standard error on species abundances (%) was calculated and used to determine confidence intervals (Patterson and Fishbein, 1989).

Stratigraphically constrained cluster analysis was conducted on samples using the R package Rioja (Juggins, 2012) using the Constrained Increment Sum of Squares (CONISS) algorithm outlined in Grimm (1987). Number and position of biofacies within clusters were determined using a broken stick model generated by Rioja. The Shannon–Weaver Diversity Index (SDI) was used as a measure of diversity within samples, as diversity often changes with environment shifts (Culver, 1990; Murray, 1991). The SDI was calculated using the paleontological freeware program PAST. Summary figures were generated using the packages Rioja and Analogue for R (Juggins, 2012; Simpson and Oksanen, 2013).

Three samples from PB02 and PC01 were radiocarbon dated (AMS) at Beta Analytic (Table 1). The samples were undifferentiated OM as no plant macrofossils were found in the sediment. Dates were calibrated using the R package Clam (Blaauw, 2010) based on the IntCal13.14C terrestrial age calibration curve (Reimer et al., 2013). An implicit date of −60 yr BP was assumed for surface samples. A smooth spline was used to generate the age-depth models. All dates are reported in calendar years before present (yr BP).

4. Results

4.1. Lithology and LOI

4.1.1. Core PB02

PB02 is composed of mud with variable OM and ranges in color from dark brown to grey. Intervals with greater organic content appear brown in color images (RGB) and darker grey in radiographic images (XRI, Fig. 2). Images show thin horizontal bedding (<1 cm) throughout the core, indicating little bioturbation. At the base of the core (330–310 cm), OM is generally low (<10%), but increases between 310 and 230 cm to values that are high and variable (~15–60%). Between 230 and 0 cm, OM values are lower (~10–20%), but increase slightly (15–20%) between 80 and 0 cm. CaCO$_3$ values are high and variable from 330 to 180 cm (~20–60%), but drop sharply between 280 and 220 cm to lower values (<10%) relative to the rest of the core. In this same interval, there are gypsum crystals several mm long and columnar in habit. Above 180 cm, CaCO$_3$ values gradually increase from 15 to 30% towards the top of the core. The silicate fraction displays an inverse trend to that of CaCO$_3$, except between 280 and 220 cm where the OM content is high.

4.1.2. Core PC01

Similar to PB02, PC01 is composed of brown to grey mud with variable amounts of OM (Fig. 3). The XRI shows mm-scale horizontal bedding with shifts in lithology closely following the OM content. OM is generally <5% from 275 to 210 cm, but increases sharply to ~8% at 210 cm, and then again at 70 cm, reaching 25% at the top of the core. CaCO$_3$ is initially <5%, but begins to increase above 225 cm and becomes more variable (10–30%) from 225 to 170 cm. This is similar to PB02, except without the drop in values (280–220 cm). Above 170 cm, CaCO$_3$ values are lower (~10%) and less variable, but gradually increase to 15% at the top of the core. The pattern of silicate values varies inversely to that of the CaCO$_3$ and OM, with a general decrease in values moving up-core.

4.2. X-ray fluorescence

Errors associated with matrix effects and dilution effects, as well as variability in sedimentary components of the core (pore water, grain size, surface roughness), makes conversion of XRF data to absolute concentrations difficult without the use of quantitative geochemical analysis of bulk sediment (Weltje and Tjallingii, 2008; Löwemark et al., 2011). We therefore report Fe, Ti, Ca, and K in counts per second (cps), which show relative variations of the elements instead of absolute concentrations. Of the elements examined in this study, Fe is most abundant,

Table 1
Radiocarbon dates and calibrated ages for Playa Bailen (core PB02) and Punta de Cartas (core PC01).

Lab ID	Sample ID	Depth (cm)	Conventional radiocarbon age	δ^{13}C (‰VPDB)	Calibrated yr BP (2σ)
Beta — 291719	PB02 115 — 116	115.5	950	−22.9	761–923
Beta — 291720	PB02 205 — 206	205.5	1950	−20	1725–1876
Beta — 291721	PB02 300 — 301	300.5	3250	−23.3	3367–3555
Beta — 291722	PC01 58 — 59	58.5	1140	−20.8	930–1054
Beta — 291723	PC01 147 — 148	147.5	1810	−21.2	1554–1810
Beta — 291724	PC01 243 — 244	243.5	2890	−22.8	2997–3247

peaking at 45,000 cps, but generally ranging from 5000 to 15,000 cps. Ti is less abundant, between 100 and 1000 cps, and K never exceeds 500 cps. In core PB02, Fe, Ti, and K correlate well with each other ($r_{K-Ti} = 0.84$; $r_{Fe-Ti} = 0.77$; $r_{Fe-K} = 0.83$) indicating all three elements are from the same source area. In core PC01, K and Fe have a strong positive correlation ($r_{Fe-K} = 0.71$), whereas Ti shows a weaker correlation with K ($r_{K-Ti} = 0.55$) and Fe ($r_{Fe-Ti} = 0.34$) which may indicate that Ti at Punta de Cartas is from a different source than K and Fe. All three elements, however, display similar variations, suggesting regional-scale processes affect material input to the lagoons.

Elements in core PB02 shows good agreement between K, Ti and Fe values (cps), except in the lower section of the core (Fig. 2). Ti values decrease between 330 and 225 cm from ~600 to 175 cps, while K decreases from ~200 to 100 cps over the same interval. In contrast, Fe values show an increase between 330 and 225 cm, starting at ~500 cps and reaching 1000 cps by 225 cm. Variations in elements are, however, more consistent through the rest of the core. Fe, Ti, and K are highly variable between 225 and 160 cm (Fe: 26523–1174 cps; Ti: 762–25 cps; K: 345–4 cps) and begin to gradually decrease above 160 cm, reaching low values at the top of the core (Fe: 2803 cps; Ti: 64 cps; K: 90 cps).

Ti/Ca is an element ratio commonly used in marine environments to examine variations in terrestrial input. In core PB02, the Ti/Ca ratio varies between 0.05 and 2 and shows a general decrease in value up-core (Fig. 2). Higher Ti/Ca values (0.2–2.0) are observed between ~275 and 225 cm and ~325 to 310 cm. These values are associated with abnormally low (<500 cps) Ca, which remains generally above

2000 cps in the rest of the core. These highs are followed by relatively stable Ti/Ca values of ~0.13 until 150 cm, above which Ti/Ca decreases, reaching 0.01 by the top of the core. The inflection points of Ti/Ca at 225 cm and 150 cm correlate with changes in the Ti, Fe and K data.

Elemental concentrations at the base of core PC01 are high at 30,000, 800, and 250 cps respectively for Fe, Ti, and K (Fig. 3), and gradually decrease to lower values at 190 cm. From 190 to 75 cm, values are variable, with several large peaks and lows (Fe: 29083–5132 cps; Ti: 1024–47 cps; K: 496–49 cps). Values show a decreasing trend from 75 cm to the core top.

The Ti/Ca ratio varies from 0.20 to 12 in core PC01, with higher values occurring near the base of the core associated with relatively low Ca (<100 cps) compared to the rest of the core (mean 865 cps, Fig. 3). Ti/Ca shows a similar trend as Fe, Ti and K in core PC01 with two periods of decreasing values between 270 and 190 cm and 75 to 9 cm bracketing an interval of high, variable Ti/Ca with a stable mean (~0.5).

4.3. Foraminifera biofacies

4.3.1. Core PB02

Samples from core PB02 contained foraminifera at most depths, excluding those at 280 cm and between 270 and 220 cm (Fig. 4). Identified species include *Elphidium excavatum*, *Elphidium poeyanum*, *Ammonia beccarii* forma *tepida*, *A. beccarii* forma *pakinsoniana*, *Quinqueloculina seminulum*, *Quinqueloculina crassa*, *Quinqueloculina bosciana*, *Triloculina oblonga*, *Triloculina schreiberiana*, *Nonionella atlantica*, *Fursenkoina* sp.,
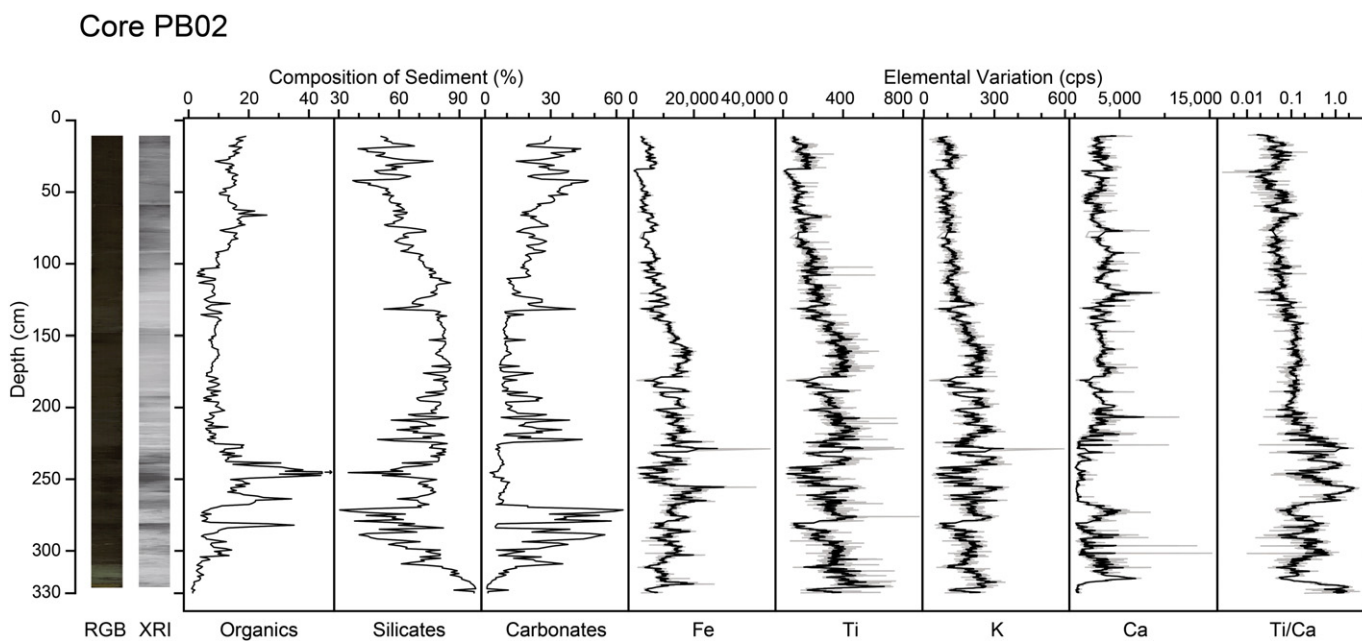
Core PB02

Fig. 2. Summary of lithologic and geochemical results for core PB02 (Playa Bailen) plotted vs depth. From left to right: RBG and XRI images, LOI results (proportion OM, CaCO₃ and silicates) reported in percentage of total sediment composition, elemental variations (cps) derived from core scanning XRF, and the Ti/Ca ratio. For the XRF data, the grey lines represent original XRF values, while the black line represents the 5-point running mean of XRF values.

Core PC01
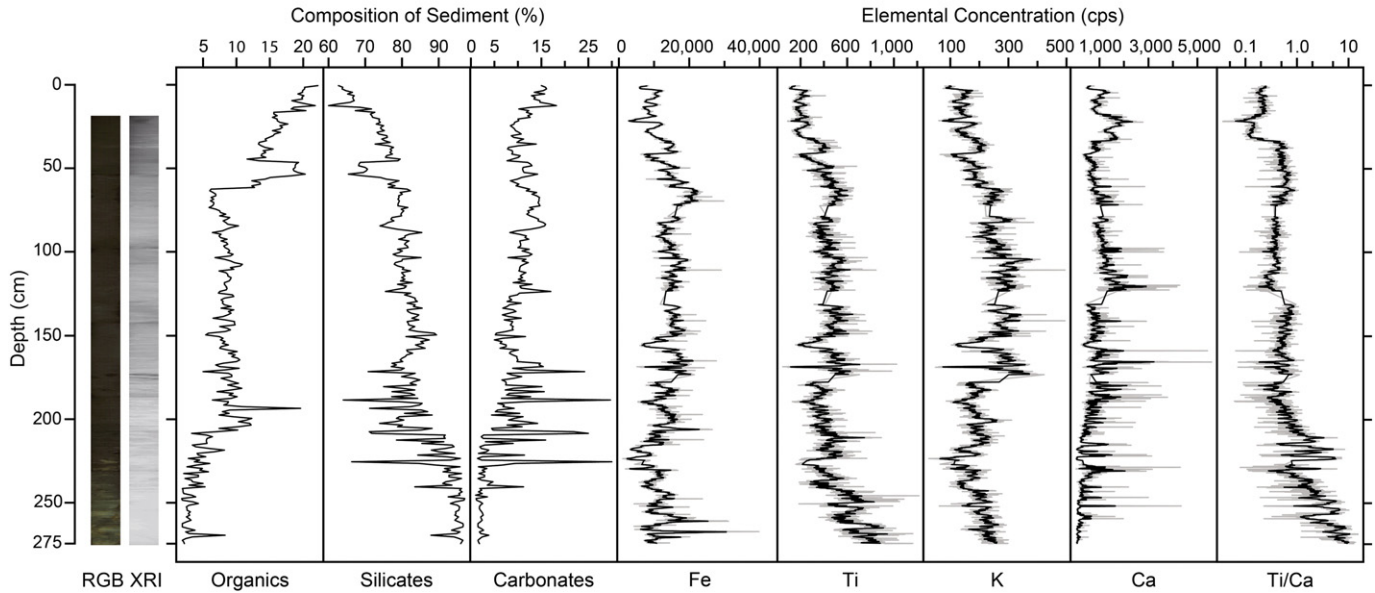
Fig. 3. Summary of lithologic and geochemical data for core PC01 (Punta de Cartas) plotted vs depth. From left to right: RBG and XRI images, LOI results (proportion OM, CaCO₃ and silicates) reported in percentage of total sediment composition, elemental variations (cps) derived from core scanning XRF, and the Ti/Ca ratio. For the XRF data, the grey lines represent original XRF values, while the black line represents the 5-point running mean of XRF values.

Polymorphina sp., and *Cornuspira involvens*. Stratigraphically constrained cluster analysis separated foraminifera species into four distinct assemblages that follow an increasing marine tendency up core.

Assemblage 1 — The *Ammonia–Quinqueloculina* (AQ) Assemblage, is found from 330 to 280 cm (Fig. 4). The AQ Assemblage is dominated by *A. beccarii* forma *tepida* (27%), *Q. seminulum* (28%), *A. beccarii* forma

Core PB02
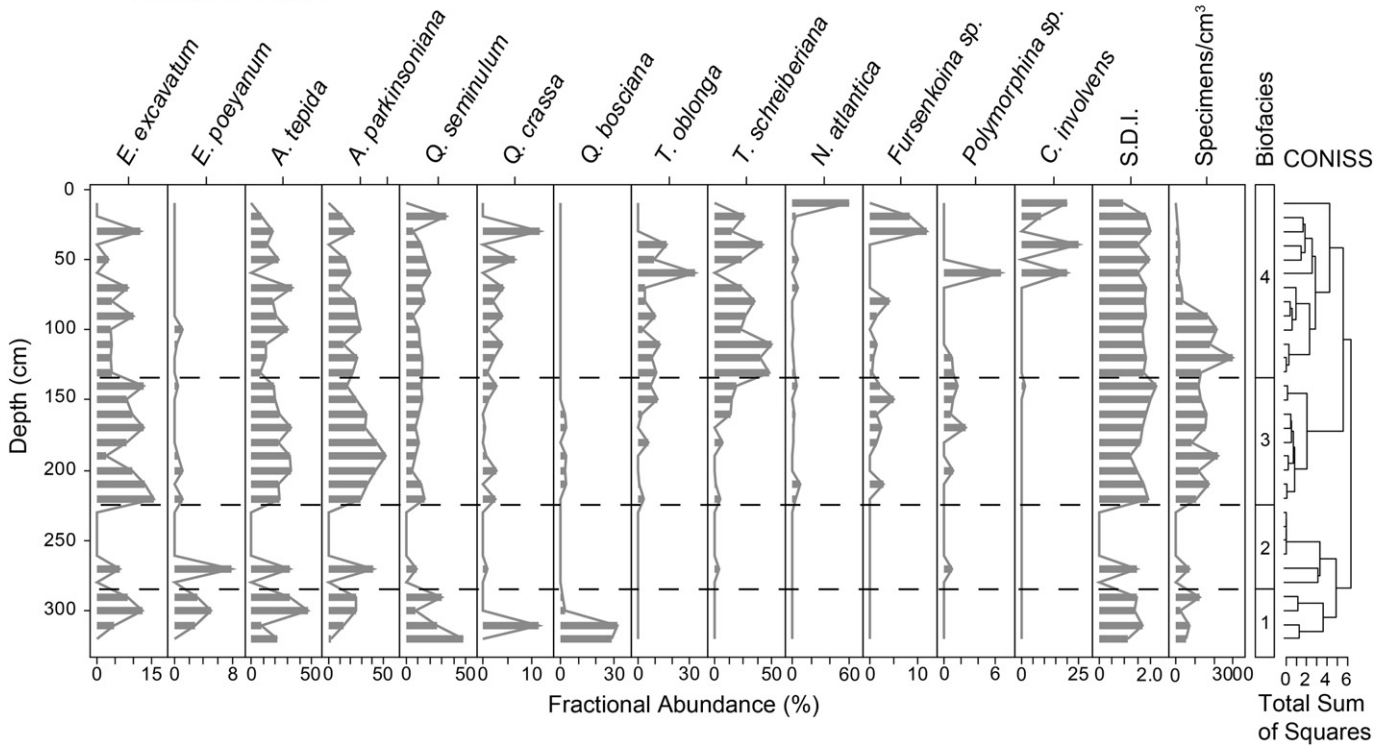
Fig. 4. Foraminifera results for Playa Bailen (PB02) plotted vs depth. From left to right: abundance of foraminifera species, diversity of a sample, total abundance of foraminifera, and biofacies inferred from CONISS results on the far right. Foraminifera are reported as a fractional abundance, sample diversity is represented by the Shannon–Weaver diversity index (SDI), and the total abundance of foraminifera as specimens/cm³. The dashed black lines separate biofacies.

parkinsoniana (17%), and *Q. bosciana* (17%). Additional species of *Quinqueloculina*, *Triloculina* and *Elphidium* were present, but were below ~10% on average. *Ammonia* species are tolerant of a range of salinity, but both *Ammonia* and *Elphidium* species are normally found in brackish environments (Murray, 1991; Hayward and Hollis, 1994; Labin et al., 1995; Debenay, 2000; Debenay and Guillou, 2002). *Quinqueloculina* and *Triloculina* are more commonly found at higher salinities between 25 and 40‰, but some species are found in brackish-marine lagoons (Culver, 1990; Murray, 1991; Hayward and Hollis, 1994; Brewster-Wingard and Ishman, 1999; Debenay, 2000; Debenay and Guillou, 2002; Gischler et al., 2003). The Shannon Diversity Index (SDI) was moderate, averaging 1.42. The species present and SDI indicate that salinity in the lagoon was near the upper limits of polyhaline (25–30‰).

Assemblage 2 — The Barren (B) Assemblage is composed of samples containing no foraminifera from 280 to 225 cm, with the exception of one sample at 270 cm that contained low amounts of *A. beccarri* forma *tepida* (Fig. 4). *Ammonia* species, particularly *A. beccarrii* forma *tepida*, are opportunistic and can tolerate abrupt salinity shifts and extreme salinities, ranging from 1 to 90‰ (Walton and Sloan, 1990; Labin et al., 1995). Gypsum crystals found in this interval may have been transported from the lagoon margin, or may reflect stagnant and possibly anoxic bottom-water conditions caused by the degradation of OM, which was prevalent during this interval. This assemblage represents a period of harsh conditions not conducive to foraminifera colonization.

Assemblage 3 — The *Ammonia* (A) Assemblage occurs between 225 and 135 cm, and consists primarily of *Ammonia* species (*A. beccarii* forma *tepida*, and forma *parkinsoniana*) with a combined average of ~55% (Fig. 4). *E. excavatum* and *Q. seminulum* are also common (~10%), among other minor species. SDI values increase to an average of 1.74 is because of an increase in minor species, prominently *Triloculina* spp. and *N. atlantica*. These species are associated with marine salinities and shelf environments, but can also be found in lagoons (Culver, 1990; Hayward and Hollis, 1994; Debenay, 2000; Gischler et al., 2003; Eichler et al., 2004; Jarecki and Walkey, 2006).

This indicates an overall increase in salinity to likely euhaline values (30–35‰).

Assemblage 4 — the *Ammonia–Triloculina* Assemblage (135–0 cm) has similar diversity to Assemblage 3 (average SDI 1.70, Fig. 4). *Triloculina* spp., although initially lower, increase above 80 cm, replacing *Ammonia* and *Quinqueloculina* as the dominant species. *Triloculina* species are associated with the upper range of marine values; notably *T. oblonga* is associated with hypersaline conditions (Murray, 1991; Debenay et al., 2001; Cheng et al., 2012). Other minor species (e.g., *Fursenkoina sp.*) also increase in abundance during this interval indicating salinities closer to euhaline (30–35‰) or perhaps slightly higher, near metahaline values (35–40‰).

4.3.2. Core PC01

Eight foraminifera species were found statistically significant in core PC01: *E. excavatum*, *E. poeyanum*, *Bolivina spathulata*, *A. beccarii* forma *tepida*, *A. beccarii* forma *parkinsoniana*, *Fursenkoina* sp., *N. atlantica*, and *Pyrgo* sp. (Fig. 5). CONISS cluster analysis revealed three assemblages that exhibit lower diversity than core PB02 (~1.5 vs ~1.75), indicating harsher, brackish conditions. A similar trend of salinity increase up-core, however, was observed.

Assemblage 1, from 260 to 200 cm depth, is similar to the Barren Assemblage observed in PB02 in that foraminifera are generally very low or absent (Fig. 5). The assemblage contains predominantly *A. beccarii* forma *tepida*, but also *Elphidium* spp., representing a brackish (polyhaline 18–30‰), possibly harsh environment.

Assemblages 2 and 3 are similar to the *Ammonia* Assemblage in PB02, and contain several other minor species, whose abundance separates Assemblages 2 and 3 (i.e., *N. atlantica*, *Pyrgo* sp., Fig. 5). Assemblage 2 ranges from 200 to 100 cm in the core, and has lower diversity (1.25) than Assemblage 3. Assemblage 3 occurs from 100 to 0 cm, and has higher abundances of minor species and slightly increased SDI (1.39), representing a shift from brackish or polyhaline conditions (18–25‰) to slightly more saline polyhaline conditions (25–35‰) towards the core-top.
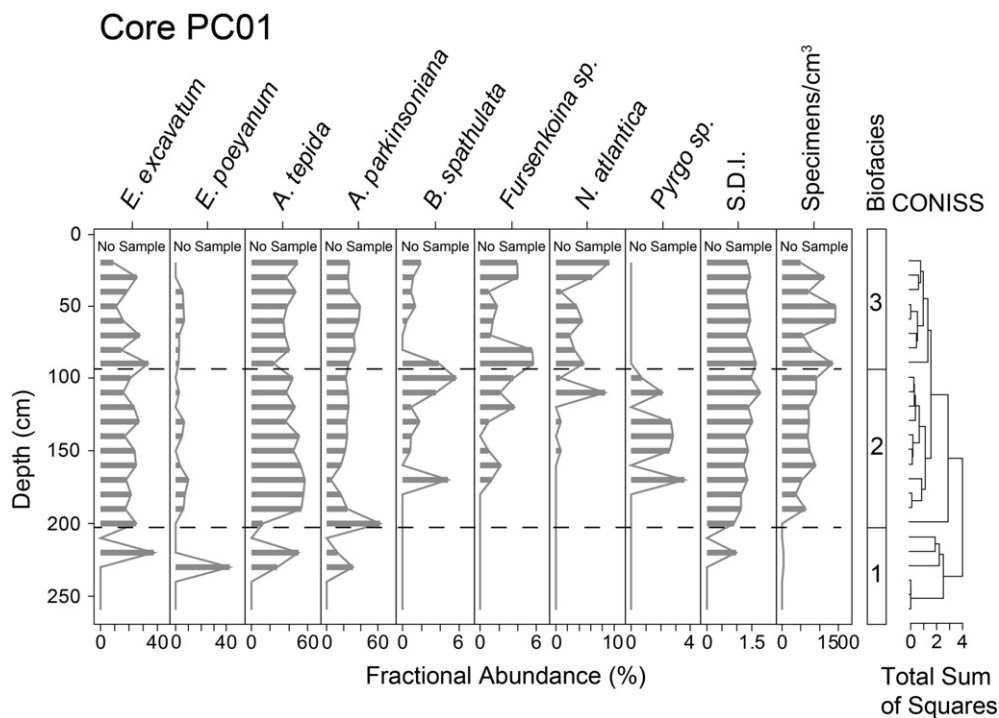
Fig. 5. Foraminifera results for Punta de Cartas (PC01) plotted vs depth. From left to right: abundance of foraminifera species, diversity of a sample, total abundance of foraminifera, and biofacies inferred from CONISS results on the far right. Foraminifera are reported as a fractional abundance, sample diversity is represented by the Shannon–Weaver diversity index (SDI), and the total abundance of foraminifera as specimens/cm³. The dashed black lines separate biofacies.
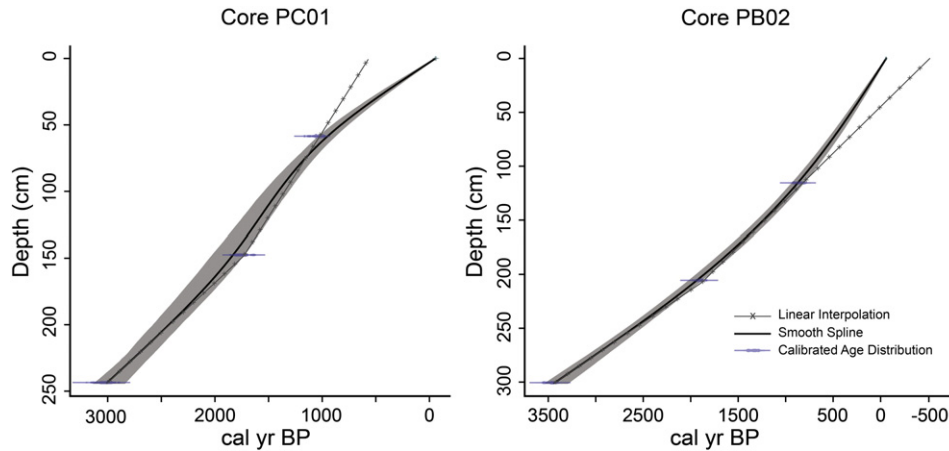
Fig. 6. Age models for cores PC01 and PB02, generated using the package CLAM for R statistical software. The black line represents the "best age" calculated as a weighted average of all iterations of age–depth models generated for this core. The grey shaded regions represent 2σ confidence interval of the best age model. The thin blue graphs, which represent dated samples, show the calibrated age distributions (calendar yr BP) for each date. The dark grey "x" line represents hypothetical extrapolation of an age model generated through linear interpolation of neighboring dates.

4.4. Chronology

The age model for PC01 is best described by an inverse cubic function, with exponential increase in linear sediment accumulation up to 110 cm, followed by a decrease to the top of the core (Fig. 6). PC01 shows greater uncertainty in its age model than PB02, increasing from ± 100 to ± 125 yrs below 50 cm. The rate of sediment accumulation in PC01 averages 0.86 mm/yr. PB02's age model shows a consistent increase in sediment accumulation up-core. Sediment accumulation rates average 1.1 mm/yr overall, with higher rates at the top of the core (Fig. 6). The error associated with the age model is approximately ± 100 yr.

Hard-water error, associated with the incorporation of older carbon sources by aquatic plants, can result in an over-estimate of the age of sediment. This commonly occurs in the dating of bulk sediment samples (Shotton, 1972; Barnekow et al., 1998; Grimm et al., 2009), which represent an agglomeration of carbon from different sources. Hard-water errors in radiocarbon dating have been observed previously in this region, notably at Laguna de la Leche, northern Cuba, where a 1600 yr correction was applied to bulk sediment samples based on the extrapolation of a linear age model to 0 cm depth (Peros et al., 2007a,b). Numerous aquatic plant macrofossils, the presence of a shell-rich marl, and limestone bedrock support the application of this correction. Conversely, Punta de Cartas and Playa Bailen show no evidence of aquatic or terrestrial macrofossils. Red Mangrove (*R. mangle*) presently dominates the surrounding vegetation. This species of mangrove thrives in brackish to marine salinities (5–35‰) in littoral environments (Smith and Snedaker, 1995). Foraminifera evidence indicate salinities best suited to red mangrove occurred at this site for the past ~4000 cal yr BP. It is expected that much of the OM in our bulk sediment samples would be derived from the mangroves that likely surrounded these lagoons since their initiation, although contamination of sediment by aquatic sources of carbon should not be ruled out. Extrapolating age models generated using linear interpolation of neighboring dates yields an offset of 588 cal yr BP ± 173 yr for core PC01 and −480 cal yr BP ± 213 yr for Core PB02 (Fig. 5, dark grey "x" lines). Despite these offsets, our data is in general agreement with other paleoclimate proxies from the circum-Caribbean (see Discussion, below), suggesting that any dating errors are relatively minor. In addition, all the dates from both cores are in chronological order (i.e., there are no inversions), lending further support to our age-depth models. As such, no correction was applied to the radiocarbon dates presented in this study, although we consider these to be tentative chronologies, as we cannot dismiss a hard water error.

5. Discussion

5.1. Foraminifera and salinity

The foraminifera data from Punta de Cartas and Playa Bailen show similar patterns of salinity shifts during the late Holocene, though the assemblages found in each lagoon differ, with Playa Bailen having a slightly higher diversity than Punta de Cartas. Both locations show trends towards relatively more marine conditions spanning the last ~3000 yr BP with similar timing in assemblage transitions (PB02: ~1100, 2300, and 3000 yr BP; PC01: ~1400, and 2500 yr BP) suggesting a regional vs basin specific effect.

At Playa Bailen, the *Ammonia–Quinqueloculina* Assemblage is found between 3000 and 4000 yr BP indicating polyhaline (18–30‰) to euhaline (30–35‰) salinities (Fig. 7). The Barren Assemblage begins at ~3000 yr BP, indicating harsher, perhaps anoxic, low-salinity conditions. The waterbody became slightly more marine after ~2300 yr BP, for instance where the *Ammonia* Assemblage indicates polyhaline salinity (25–30‰). These conditions continue until ~1400 yr BP, when the foraminiferal assemblage transitions to the higher-diversity *Ammonia–Triloculina* assemblage, indicating more marine salinities in the euhaline to metahaline range (30–40‰), which continued to present.

Punta de Cartas shows a similar pattern. The Barren assemblage also occurs at Punta de Cartas, albeit earlier than observed at Playa Bailen, beginning at ~3500 yr BP, but terminates at about the same time it ended in Playa Bailen, at ~2500 yr BP (Fig. 8). The relatively more marine *Ammonia* Assemblage is found in the lagoon until 1500 yr BP when an increase in the concentration of minor species marks the shift to slightly more saline values, in the upper range of polyhaline (25–30‰).

A sediment record from Laguna de la Leche, on the north-central coast of Cuba, shows salinity shifts similar to those from Playa Bailen and Punta de Cartas, although the timing is slightly different. This may be a consequence of age uncertainties in Laguna de la Leche as a 1600-yr correction was applied to the radiocarbon dates (Peros et al., 2007a, b). In Laguna de la Leche, the transition from brackish to marine conditions was demarcated by the transition from an *Ammonia* biofacies to one containing *Elphidium* spp. and *T. oblonga*, which occurred after ~3200 yr BP. The ^{87}Sr/^{86}Sr values from *Ammonia* tests, however, indicated marine conditions occurring after 2700 yr BP (Peros et al., 2007a), and palynological results showed a shift to higher salinity over the past 1400 yr BP, with an increase in *R. mangle* (red mangrove) and *Conocarpus erectus* (buttonwood mangrove) pollen (Peros et al., 2007b). Although there is a differences in the timing, and likely the
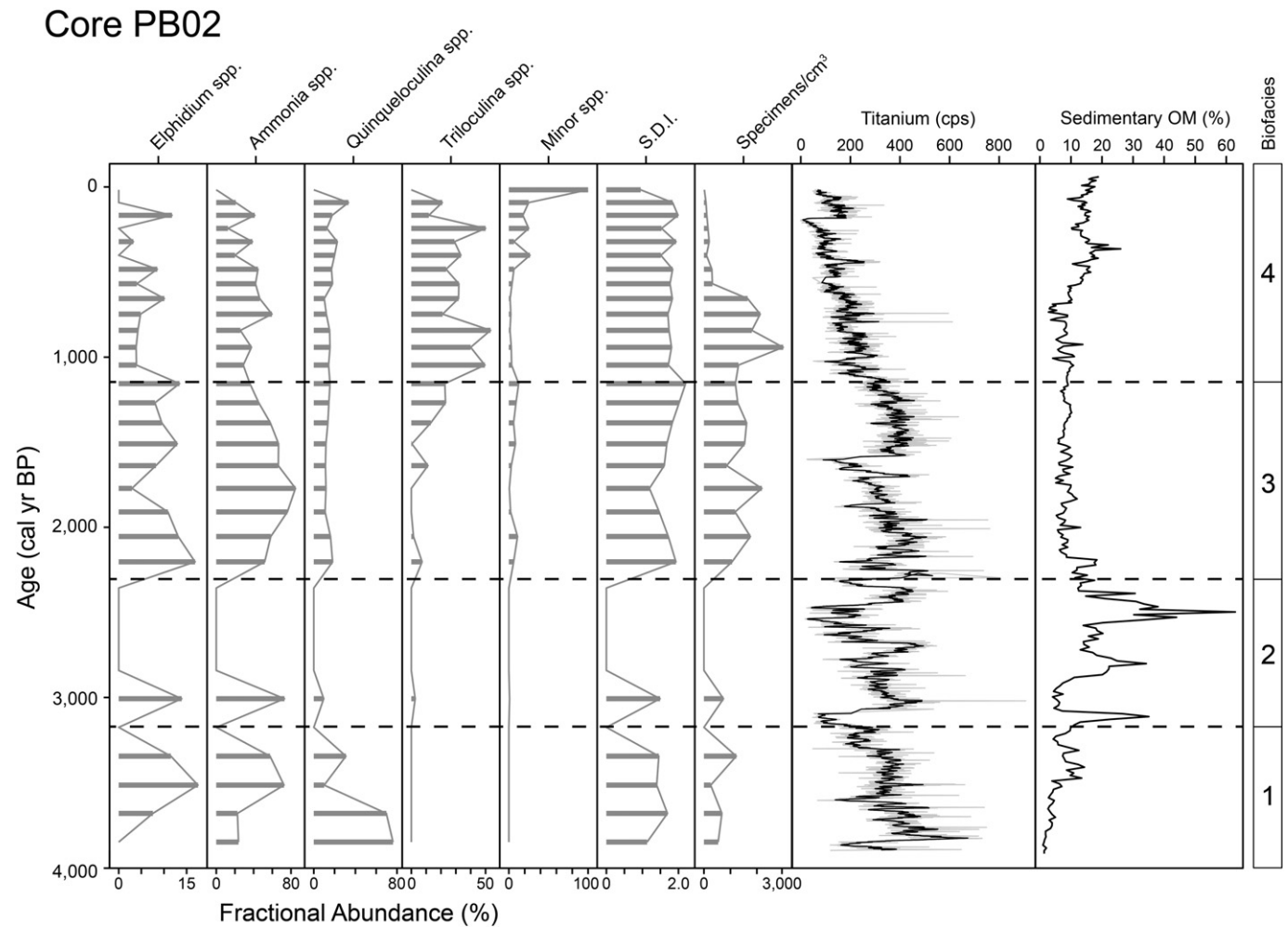
Fig. 7. Summary of microfossil data, XRF-derived terrigenous inputs (Ti), foraminifera, OM (%) and biofacies at Playa Bailen (PB02) relative to age (yr BP). Foraminifera are grouped by genus and represented as fractional abundance. Ti (cps) represents terrigenous input to the lagoon. Biofacies are demarcated by dashed lines.

sensitivity, of the different proxies, an overall tendency towards more marine salinities (30–35‰) over the last ~3500 yr BP at Playa Bailen, Punta de Cartas, and Laguna de la Leche suggests regional-scale forcing of salinity in Cuban lagoons.

5.2. Sea level and lagoon evolution

Coring in Playa Bailen and Punta de Cartas terminated on grey clay likely deposited in earlier pond environments, which are common features on Caribbean islands (Pilarczyk and Reinhardt, 2012). It may, alternatively, represent an intertidal mudflat formed when initial sea-level-rise flooded the terrestrial surface. Cores PB02 and PC01 suggest that the onset of marine-influenced conditions occurred by ~4000 yr BP as the water depth (~70 cm) and the core length at Play Bailen and Punta de Cartas, 330 cm and 275 cm respectively, correspond with Caribbean sea-level curves (i.e., − 3.5 to − 2.75 masl at 4000 yr BP; Milne and Peros, 2013; Toscano and Macintyre, 2003). Lithologic characteristics are relatively constant throughout cores PC01 and PB02, suggesting sedimentation kept pace with sea-level-rise, and water depth within the lagoons varied little during the period of the record. The radiocarbon age model indicates relatively constant sedimentation, and the XRI reinforces this interpretation, as the sediments have thin beds (~1–5 mm) and show minimal bioturbation. There are trends in sediment composition (OM, CaCO₃, and silicates), but these are fairly minor, varying for the most part by only 10–20%.

Constant sedimentation, its muddy, OM-rich texture, and the undisturbed bedding indicate that the barrier was emplaced by at least 4000 yr BP, and likely formed shortly after sea-level reached its present height. The lack of coarse sand intervals or sedimentary structures in the cores suggests that the barrier has not been modified significantly throughout its history. The foraminiferal data do not indicate any short-term changes in salinity associated with opening and closing of the barrier, and the collective evidence indicates a slowly rising sea-level, with constant water depth (~0.5–1 m) in an enclosed lagoon.

5.3. XRF data and precipitation

The amount of terrigenous input, inferred from Fe, Ti, K and the Ti/Ca ratio, has been used as a paleo-rainfall proxy in open marine basins and shelves previously (e.g., Haug et al., 2001). Elemental ratios serve to normalize data, minimizing matrix effects (Zabel et al., 2001; Jaeschke et al., 2007; Bender et al., 2013; Burone et al., 2013). Ti/Ca and Fe/Ca are often used to document terrigenous input to coastal shelves and deep basins. In offshore environments, Ca remains relatively stable in comparison to littoral systems, where changes in the geomorphology and productivity of sedimentary basins have a greater influence on the Ca proportion in sediment. In core PB02, low Ca values near the base of the core bias Ti/Ca results to higher values. If these high Ti/Ca values were a consequence of greater precipitation, there should be an observed response in the Fe, Ti and K records. These elements, however,
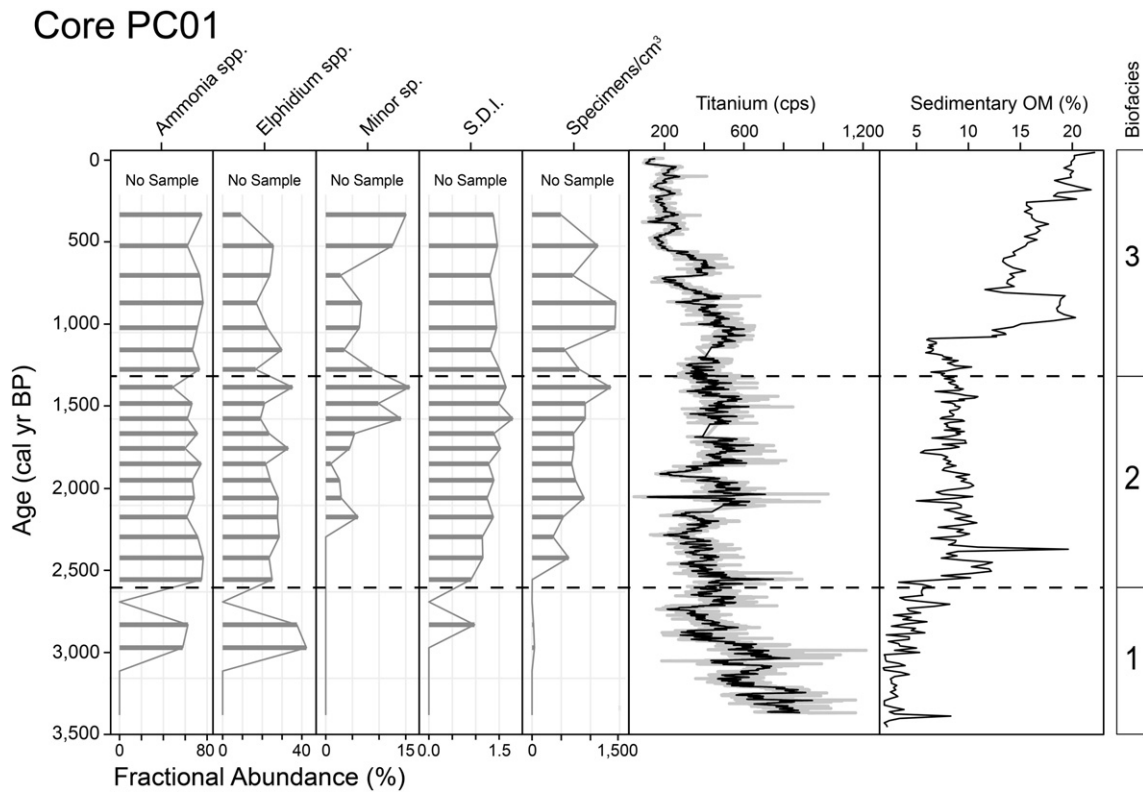
Fig. 8. Summary of microfossil data, XRF-derived terrigenous inputs (Ti), foraminifera, OM (%) and biofacies at Punta de Cartas relative to age (yr BP). Foraminifera are grouped by genus and reported as fractional abundance. Ti (cps) represents terrigenous input to the lagoon. Biofacies are demarcated by dashed lines.

remain stable during this interval. Stable erosional inputs and decreasing Ca may, alternatively, be caused by dilution, yet no other elements show a decrease during this interval, which would be expected if high Ti, Fe and K input rates were diluting other elements. This suggests elevated Ti/Ca values near the base of the core are not related to a precipitation signal, but instead to other variables. Similarly, low Ca counts influence Ti/Ca values in core PC01, though the effect is less obvious. Despite the bias resulting from variable Ca, the Ti/Ca record shows similar trends as Ti, Fe and K. Because of possible uncertainties in attributing Ti/Ca ratios to precipitation, and given the similar timing among the variations of Ti, Fe, K and the Ti/Ca ratio, single-element records are discussed hereafter.

If the lagoon water depth and barrier morphology remained relatively constant, as argued above, then precipitation should have had a strong control on salinity within the lagoon. Overall, Ti shows the best relationship with the foraminifera-based salinity reconstructions, with an overall decreasing trend in values (cps) up-core in both Playa Bailen and Punta de Cartas. PB02 has Ti values of 400 cps at 4000 yr BP and 100 cps at the top of the core, with a distinctive decline beginning at 1200–1100 yr BP (Fig. 7). PC01 shows a similar pattern. Ti values decrease from 700 cps at 3500 yr BP to 200 cps at present, with a flexion point at 1200–1100 yr BP (Fig. 8). K and Fe values follow the same pattern in both cores.

Matrix effects and dilution effects associated with core-scanning XRF may confound determination of elemental concentrations (Löwemark et al., 2011). Notably, increases in proportion of lighter elements associated with OM can significantly reduce cps, causing erroneously low values. Crossplots of XRF data (Ti, Fe and K) show there is a weak negative relationship between trace elements and OM, indicated by r values <0.30; Ti in core PC01 is an exception showing a moderate negative relationship with OM (r = −0.6066, Fig. 9). Increases in OM (from ~10 to 20%) in the last ~1400–1200 yr BP occur alongside decreases in Ti, Fe and K. The magnitude of the change in OM, however, is not concomitant with the change in elemental concentration (Figs. 7, 8). In the PB02,

record there is a large increase in OM from 3000 to 2300 yr BP, but this had little effect on variations in the elements. The decrease in silicates or terrigenous input at ~1200–1400 yr BP also would be expected with decreasing freshwater input to the lagoon. The increase in salinity recorded by the foraminifera, and the decrease in Ti, Fe, and K, indicate drier conditions with less freshwater discharge entering both Playa Bailen and Punta de Cartas since ~1400–1200 yr BP.

5.4. Caribbean precipitation trends

5.4.1. Coastal and shelf records

Inferences for higher salinity and decreased terrigenous input after ~1400–1200 cal yr BP match other paleoclimate records from the Caribbean and indicate increasingly arid conditions during the late Holocene. At Grand Case pond, St. Martin, an increase in evaporites occurred from 4500 to 2350 yr BP and after 1100 yr BP, indicating drier conditions (Malaizé et al., 2011). Mg/Ca paleothermometry of foraminifera from the Cariaco Basin show a sea-surface temperature decrease after 1200 yr BP (Wurtzel et al., 2013). On the western coast of the Yucatan Peninsula, shifts in mangrove species indicate drier conditions after 1500 yr BP (Islebe and Sanchez, 2002). Pollen and geochemical data from a core taken in the back-barrier lagoon of Turneffe Atoll, Belize, imply an increasingly saline environment from 4000 to 3000 yr BP and from 2000 yr BP until present, likely related to reduced precipitation (Wooller et al., 2009). XRF-derived Ti from Laguna Playa Grande, Vieques, Puerto Rico, shows an abrupt increase at ~1400 yr BP, indicating increased precipitation, whereas Cuban lagoon records indicate increased aridity during this period (Woodruff et al., 2008). Hurricane records from the same study area, however, show decreased activity for the same period (Donnelly and Woodruff, 2007; Woodruff et al., 2008). Frequent hurricane strikes would likely result in greater erosion and transport of sediment, increasing Ti input to the lagoon. It is possible that the Ti record at Laguna Playa Grande represents a response to variables other than precipitation, such as changes in
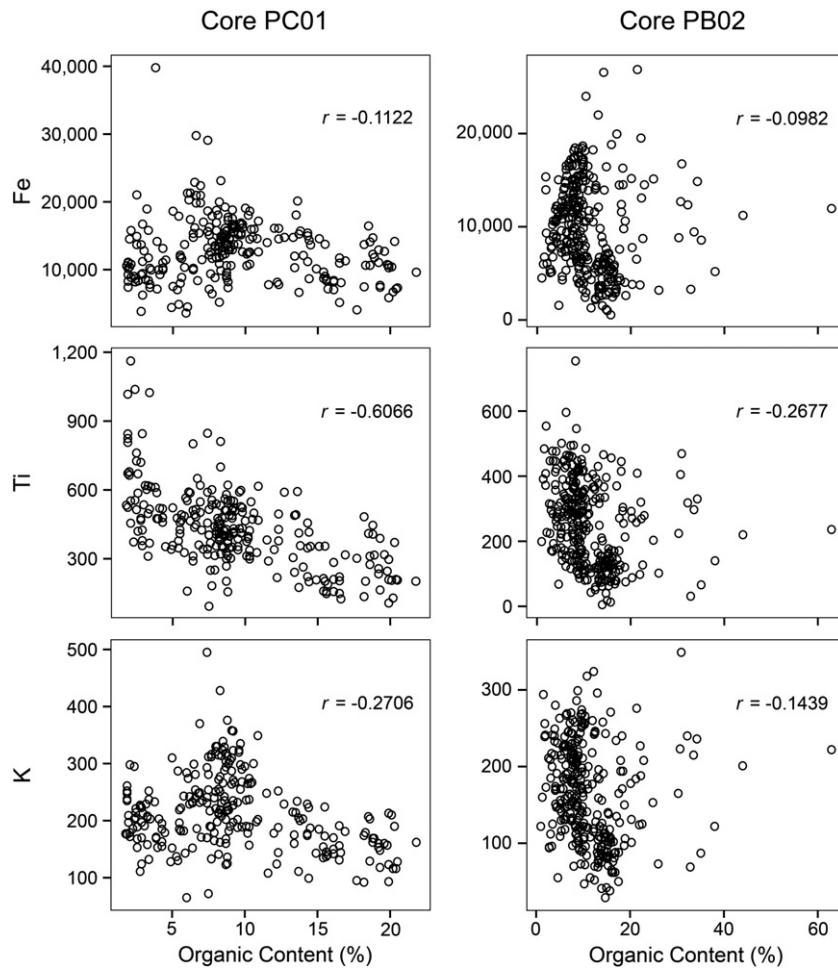
Fig. 9. Crossplots of trace element data (Ti, Fe and K in cps) vs. OM (%) for core PB02 (right) and core PC01 (left). The r values for each graph are displayed in the upper right corner and represent the correlation between the two variables.

lagoon geomorphology, or dilution of terrestrial Ti by hurricane-induced overwash, that are unique to this site. Ti and Fe in sediment cores from the Cariaco Basin in the Southern Caribbean Sea decrease from 6000 yr BP until present, indicative of a drier late Holocene (Haug et al., 2001, Fig. 10). This trend is interrupted by a period of relatively stable values from 2400 to 800 yr BP, after which values again decrease. The inflection point, indicating increasingly dry conditions, correlates with the Cuban trace element data, supporting a regional response to climate.

5.4.2. Lacustrine records

Lacustrine records also show evidence of increased circum-Caribbean aridity in the late Holocene. At Laguna Castilla in the Cordillera Central, Dominican Republic, Lane et al. (2009, 2014) measured oxygen isotopes and found a general increase in aridity from 1500 to 900 yr BP. Diatom and other evidence from sediment cores taken from crater lakes in Grenada indicates lower lakes levels from 1600 to 1400, and 1200 to 600 yr BP, reflecting increased aridity (Fritz et al., 2011). Oxygen isotopes from a core collected in Lake Chichancanab in the center of the Yucatan Peninsula show a general drying trend from 3000 yr BP until present, with a period of intense dryness occurring between 1500 and 1000 yr BP, followed by relatively stable, dry conditions (Hodell et al., 1995). At Aguada X'caamal, on the northwest Yucatan Peninsula, oxygen isotopes and microfossil evidence indicate increasing dryness after 3000 yr BP; this trend abruptly increases between 800 and 0 yr BP (Hodell et al., 2005). At Lake Punta Laguna, on the northeast Yucatan Peninsula, a period of intense dry conditions (1800–1000 yr BP) was observed in an oxygen isotope record

derived from ostracod carapaces, followed by a period of more stable, relatively wet conditions until present (Curtis et al., 1996), differing from the precipitation trend inferred from our record. In northwestern Petén, Guatemala, decreasing Ti and variations in the proportion of smectite–chlorite and halloysite in sediment cores from Laguna Tuspán indicate decreasing precipitation over the last ~6000 yr BP (Fleur et al., 2014). An increase in the amount of halloysite, and low, stable Ti values from ~1200 yr BP to present, suggests increased aridity in this region, although the coeval abandonment of the surrounding area by the local Mayan populace may alternatively have caused this trend. Sediment records from Laguna Pallcacocha in southern Ecuador also indicate a period of reduced precipitation from 2300 to 1800 yr BP, bracketed by wetter conditions; the wet phases inferred from Laguna Pallcacocha represent evidence of El Niño Southern Oscillation (ENSO) events (Moy et al., 2002). ENSO has been correlated to drier conditions in the Caribbean (Enfield and Alfaro, 1999; Giannini et al., 2001) and is known to interfere with hurricane development in the Atlantic (Gray, 1984). Hurricane records from Puerto Rico, to the southeast of Cuba, show decreased hurricane intensity from 1000 yr BP to present, correlating both with our precipitation data, and the Ecuadorian ENSO record (Donnelly and Woodruff, 2007).

5.4.3. Possible cause of precipitation variability

Southward migration of the inter-tropical convergence zone (ITCZ) can explain the precipitation trends observed at Playa Bailen and Punta de Cartas. The ITCZ is a zone of high convection caused by the convergence of trade winds north of the equator (Krishnamurti et al., 2013), and is responsible for a large portion of Caribbean precipitation.
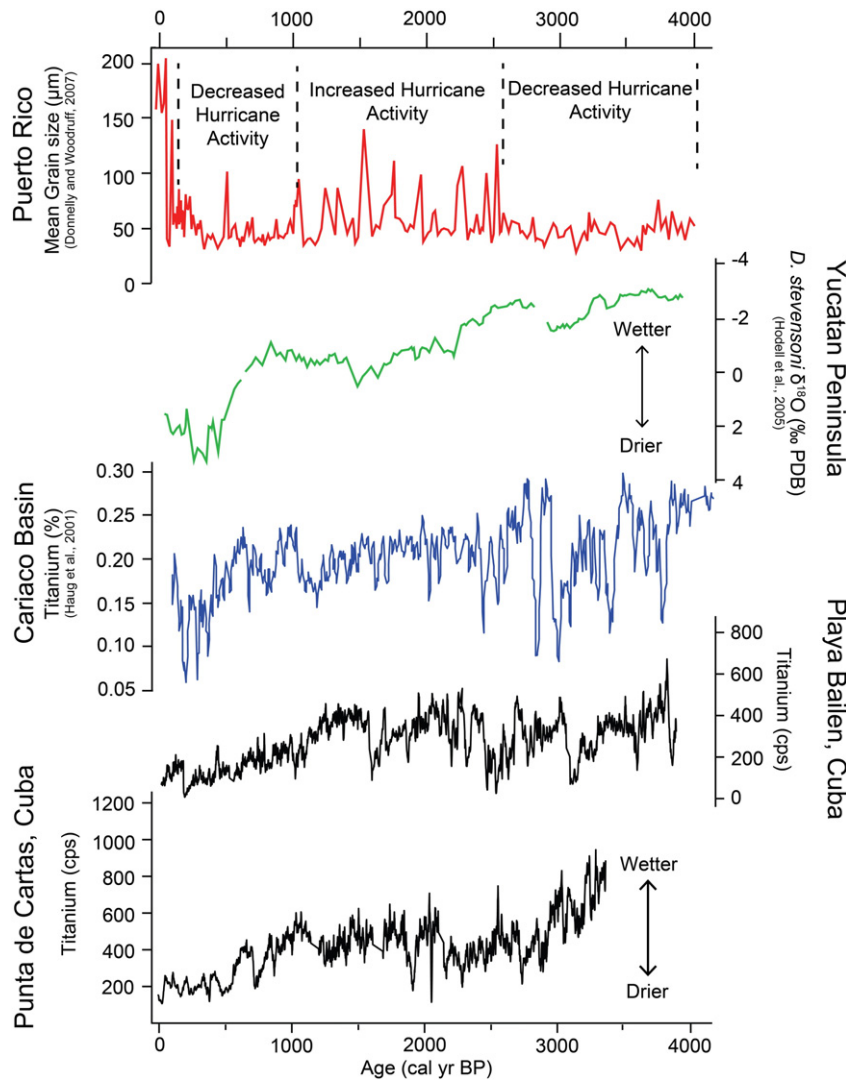
Fig. 10. Comparison of Ti data from this study to other climate proxies from the circum-Caribbean. (Red) Hurricane record from Playa Grande, Puerto Rico, with abrupt increases in mean grain size representing hurricane events (modified from Donnelly and Woodruff, 2007). (Green) δ¹⁸O (‰ PDB) record from Aguada X'caamal derived from ostracod (*D. stevensoni*) tests. Higher δ¹⁸O indicates drier conditions (modified from Hodell et al., 2005). (Blue) Ti % from Cariaco Basin sediments off the northern coast of Venezuela; higher Ti indicates wetter conditions (modified from Haug et al., 2001). (Black) Ti record (5-point running mean in cps) from Playa Bailen and Punta de Cartas, Cuba. Lower cps represent drier conditions.

A more southerly position of the ITCZ has been used to explain reduced late Holocene precipitation in the Caribbean, inferred from several other records (Haug et al., 2001; Malaizé et al., 2011). North–south variations in the ITCZ position may also account for the observed latitudinal discrepancies in onset of arid conditions across the Caribbean. Proxy records from sites closer to northern South America show an increase in aridity somewhat later (~1000–500 yr BP) than those from more northerly locations (~1500–1100 yr BP). Differences in the onset of aridity may also be related to a southward shift of the Bermuda High, associated with southerly ITCZ position, which forces hurricane paths southward (McCloskey and Keller, 2009; Malaizé et al., 2011). Differences in the timing of precipitation trends between Cuba and elsewhere in the Circum-Caribbean are partially explained by the shifting position of the ITCZ. Although the ITCZ may be the dominant control on precipitation in Cuba, correlations to hurricane activity and ENSO frequency suggest additional variables also influence Cuban precipitation. More data from Cuba and the surrounding area are needed to fully explain variability in Caribbean precipitation patterns.

6. Conclusions

We used a combination of foraminifera and XRF elemental data from cores taken in two Cuban lagoons to reconstruct both lagoon salinity and precipitation, enabling us to infer climate patterns in Cuba during the late Holocene. A clear increase in salinity and decrease in erosional inputs (Ti, Fe, K, Ti/Ca) at ~1400–1200 yr BP indicates the onset of arid conditions in the Caribbean, as shown in previous studies. Differences in the timing of initiation of aridity may be a consequence of local influences, errors associated with core chronology, or differences in the response of multiple climate proxies to forcing in the terrestrial, littoral and marine realms. Temporal correlation of other Caribbean paleoclimate records with our trace element and foraminifera data, suggests that trends observed in Playa Bailen and Punta de Cartas were controlled by regional climate, likely associated with shifts in the position of the ITCZ. Study of other lagoons in Cuba will be used to test this assertion.

This study demonstrates the applicability of trace element analysis, using XRF core scanning, to lagoon sediments. Coupling the elemental data, which reflect terrigenous flux, with a paleosalinity proxy (e.g., foraminifera), enables assessment of past precipitation and its effect on the lagoons. If the basin has been geomorphically stable over time, as determined using microfossil and lithologic data, XRF can yield useful data for paleoclimate inference, particularly in areas where other paleoclimate archives are not available.

References

Arz, H.W., Pätzold, J., Wefer, G., 1998. Correlated millennial-scale changes in surface hydrography and terrigenous sediment yield inferred from last-glacial marine deposits off north-eastern Brazil. Quat. Res. 50, 157–166.

Barnekow, L., Possnert, G., Sandgren, P., 1998. AMS ^{14}C chronologies of Holocene lake sediments in the Abisko area, northern Sweden — a comparison between dated bulk sediment and macrofossil samples. J. Geol. Soc. Sweden (GFF) 120, 59–67.

Battistion, G.A., Gerbasi, R., Degetto, S., Sbrignadello, G., 2003. Heavy metal speciation in coastal sediments using total-reflection X-ray fluorescence spectrometry. Spectrochim. Acta 48B, 217–221.

Bender, V.B., Hanebuth, T.J.J., Chiessi, C.M., 2013. Holocene shifts of the subtropical shelf front of southeastern South America controlled by high and low latitude atmospheric forcings. Paleoceanography 28, 481–490.

Bertrand, S., Hughen, K., Pantoja, S., Sepulveda, J., Lange, C., 2007. Late Holocene climate variability of Northern Patagonia reconstructed by a multi-proxy analysis of Chilean fjord sediments (44-47 S). Geophys. Res. Abstr. 9.

Blaauw, M., 2010. Methods and code for "classical" age-modelling of radiocarbon sequences. Quat. Geochronol. 5, 1047–1059.

Braconnot, P., Harrison, S.P., Kageyama, M., Bartlein, P.J., Masson-Delmonte, V., Abe-Ouchi, A., Otto-Bliesener, B., Zhao, Y., 2012. Evaluation of climate models using palaeoclimatic data. Nat. Clim. Chang. 2, 417–424.

Brewster-Wingard, G.L., Ishman, S.E., 1999. Historical trends in salinity and substrate in central Florida Bay: a paleoecological reconstruction using modern analogue data. Estuaries 22, 369–383.

Burone, L., Ortega, L., Franco-Fraguas, P., Mahiques, M., Garcia-Rodriguez, F., Vanturini, N., Marin, Y., Brugnoli, E., Nagai, R., Muniz, P., Bicego, M., Figueira, R., Salaroli, A., 2013. A multiproxy study between the Rio de la Plata and the adjacent South-western Atlantic inner shelf to assess the sediment footprint of river vs. marine influence. Cont. Shelf Res. 55, 141–154.

Cann, J.H., Cronin, T., 2004. An association of benthic foraminifera and gypsum in Holocene sediments of estaurine Chesapeake Bay, USA. The Holocene 4, 614–620.

Cann, J.H., Bouman, R.P., Bernett, E.J., 2000. Holocene foraminifera as indicators of relative estaurine-lagoonal and oceanic influences in estuarine sediments of the River Murray, South Australia. Quat. Res. 53, 378–391.

Cheng, J., Collins, L.S., Holmes, C., 2012. Four thousand years of habitat change in Florida Bay as indicated by benthic foraminifera. J. Foraminifer. Res. 42, 3–17.

Culver, S., 1990. Benthic foraminifera of Puerto Rican mangrove-lagoon systems: potential for paleoenvironmental interpretations. PALAIOS 5, 34–51.

Curtis, J.H., Hodell, D.A., Brenner, M., 1996. Climate variability on the Yucatan Peninsula (Mexico) during the past 3500 years, and implications for Maya cultural evolution. Quat. Res. 47, 37–47.

Dean, W.E., 1974. Determination of carbonate and organic matter in calcareous sediments and sedimentary rocks by loss on ignition: comparison with other methods. J. Sediment. Petrol. 44, 242–248.

Debenay, J.P., 2000. Foraminifers of paralic tropical environments. Micropaleontology 46, 153–160.

Debenay, J.P., Guillou, J.J., 2002. Ecological transitions indicated by foraminiferal assemblages in paralic environments. Estuaries 25, 1107–1120.

Debenay, J.P., Geslin, E., Eichler, B.B., Duleba, W., Sylvestre, F., Eichler, P., 2001. Foraminiferal assemblages in a hypersaline lagoon, Araruama (R.J.), Brazil. J. Foraminifer. Res. 31, 133–151.

Donnelly, J.P., Woodruff, J.D., 2007. Intense hurricane activity over the past 5000 years controlled by El Nino and the West African monsoon. Nature 447, 465–468.

Eichler, P.P.B., Castelão, G.P., Pimenta, F.M., Eichler, B.B., de Miranda, L.B., Rodrigues, A.R., Pereira, E.R.M., 2004. Foraminifera and thecamoebians as indicator of hydrodynamic process in a choked coastal lagoon, Laguna Estaurine System, SC, Brazil. J. Coast. Res. 39, 1144–1148.

Enfield, D.B., Alfaro, E.J., 1999. The dependence of Caribbean rainfall on the interaction of the Tropical Atlantic and Pacific Oceans. J. Clim. 12, 2093–2103.

Engstrom, D.R., Wright, H.E., 1984. Chemical stratigraphy of lake sediments as a record of environmental change. In: Hawthorn, E.Y., Lund, J.W.G. (Eds.), Lake Sediments and Environmental History. University of Minnesota Press, Minnesota, pp. 11–67.

Fatela, F., Taborda, R., 2002. Confidence limits of species proportions in microfossil assemblages. Mar. Micropaleontol. 45, 169–174.

Fensterer, C., Scholz, D., Hoffman, D.L., Spötl, C., Schröder-Ritzrau, A., Horn, C., Pajón, J.M., Mangini, A., 2013. Millenial-scale climate variability during the last 12.5 ka recorded in a Caribbean speleothem. Earth Planet. Sci. Lett. 361, 143–151.

Fleur, S., Malaizé, B., Giraudeau, J., Galop, D., Bout-Roumazeilles, V., Martinez, P., Charlier, K., Carbonel, P., Arnauld, M.-C., 2014. Impacts of Mayan land use on Laguna Tuspán watershed (Petén, Guatemala), as seen through clay and ostracod analysis. J. Archaeol. Sci. 49, 372–382.

Frappier, A.B., Pyburn, J., Pinkey-Drobnis, A.D., Wang, Xianfeng, Bornett, D.R., Dahlin, B.H., 2014. Two millennia of tropical cyclone-induced mud layers in a northern Yucatán stalagmite reveal multiple overlapping climatic hazards during the Maya Terminal Classic 'megadroughts'. Geophys. Res. Lett. 41, 5148–5157.

Fritz, S.C., Björk, S., Rigsby, C.A., Baker, P.A., Calder-Church, A., Conley, D.J., 2011. Caribbean hydrological variability during the Holocene as reconstructed from crater lakes on the island of Grenada. J. Quat. Sci. 26, 829–838.

Gabriel, J.J., Reinhardt, E.G., Peros, M.C., Davidson, D.E., van Hengstum, P.J., Beddows, P.A., 2008. Palaeoenvironmental evolution of Cenote Aktun Ha(Carwash) on the Yucatan Peninsula, Mexico and its response to Holocene sea-level rise. J. Paleolimnol. 42, 199–213.

Giannini, A., Chiang, J.C.H., Cane, M.A., Kushnir, Y., Seager, R., 2001. The ENSO teleconnection to the Tropical Atlantic Ocean: contributions of the remote and local SSTs to rainfall variability in the Tropical Americas. J. Clim. 14, 4530–4544.

Gischler, E., Storz, D., 2009. High-resolution windows into Holocene climate using proxy data from Belize corals (Central America). Palaeobiodivers. Palaeoenviron. 89, 211–221.

Gischler, E., Hauser, I., Heinrich, K., Scheitel, U., 2003. Characterization of depositional environments in isolated carbonate platforms based on benthic foraminifera, Belize, Central America. PALAIOS 18, 236–255.

Gray, W.M., 1984. Atlantic seasonal hurricane frequency. Part 1: El Nino and 30 mb quasi-biennial oscillation influences. Mon. Weather Rev. 112, 1649–1668.

Grimm, E.C., 1987. CONISS: a FORTRAN 77 program for stratigraphically constrained cluster analysis by the method of incremental sum of squares. Comput. Geotech. 13, 13–35.

Grimm, E.C., Maher Jr., L.J., Nelson, D.M., 2009. The magnitude of error in conventional bulk-sediment radiocarbon dates from central North America. Quat. Res. 72, 301–308.

Haberzettl, T., Kück, B., Wulf, S., Anselmetti, F., Arizetgui, D., Corbella, H., Fey, M., Janssen, S., Lücke, A., Mayr, C., Ohlendorf, C., Schábitz, F., Schleser, G.H., Wille, M., Zolitschka, B., 2008. Hydrological variability in southeastern Patagonia and explosive volcanic activity in the southern Andean Cordillera during Oxygen Isotope Stage 3 and the Holocene inferred from lake sediments of Laguna Potrok Aike, Argentina. Palaeogeogr. Palaeoclimatol. Palaeoecol. 259, 213–229.

Haug, G.H., Hughen, K.A., Sigman, D.M., Peterson, L.C., Röhl, U., 2001. Southward migration of the intertropical convergence zone through the Holocene. Science 293, 1304–1308.

Haug, G.H., Günther, D., Peterson, L.C., Sigman, D.M., Hughen, K.A., Aeschlimann, B., 2003. Climate and the collapse of Maya civilization. Science 299, 1731–1735.

Hayward, B., Hollis, J., 1994. Brackish foraminifera in New Zealand: a taxonomic and ecologic review. Micropaleontology 40, 185–222.

Heiri, O., Lotter, A.F., Lemcke, G., 2001. Loss on ignition as a method for estimating organic and carbonate content in sediments: reproducibility and comparability of results. J. Paleolimnol. 25, 101–110.

Higuera-Gundy, A., Brenner, M., Hodell, D.A., Curtis, J.H., Leyden, B.W., Binford, M.W., 1999. A 10,300 ^{14}C yr record of climate and vegetation change from Haiti. Quat. Res. 52, 159–170.

Hodell, D.A., Curtis, J.H., Jones, G.A., Higuera-Gundy, A., Brenner, M., Binford, M.W., Dorsey, K.T., 1991. Reconstruction of Caribbean climate change over the past 10,500 years. Lett. Nat. 352, 790–793.

Hodell, D.A., Curtis, J.H., Brenner, M., 1995. Possible role of climate in the collapse of Classic Maya civilization. Lett. Nat. 375, 391–394.

Hodell, D.A., Brenner, M., Curtis, J.H., Medina-González, R., Can, E.I.-C., Albornaz-Pat, A., Guilderson, T.A., 2005. Climate change on the Yucatan Peninsula during the Little Ice Age. Quat. Res. 63, 109–121.

Holmes, J.A., Street-Perrott, F.A., Ivanovich, M., Perrott, R.A., 1995. A late Quaternary paleolimnological record from Jamaica based on trace-element chemistry of ostracod shells. Chem. Geol. 124, 143–160.

Islebe, G., Sanchez, O., 2002. Hisotry of late Holocene vegetation at Quintana Roo, Caribbean coast of Mexico. Plant Ecol. 160, 187–192.

Iturralde-Vinent, M.A., 1994. Cuban geology: a new plate-tectonic synthesis. J. Pet. Geol. 17, 39–70.

Jaeschke, A., Rühlemann, C., Arz, H., Heil, G., Lohmann, G., 2007. Coupling of millennial-scale changes in sea surface temperature and precipitation off the northeastern Brazil with high-latitude climate shifts during the last glacial period. Paleoceanography 22 (PA4206).

Jarecki, L., Walkey, M., 2006. Variable hydrology and salinity of salt ponds in the British Virgin Islands. Saline Systems 2, 2.

Javaux, E., Scott, D., 2003. Illustration of modern benthic foraminifera from Bermuda and remarks on distribution in other subtropical/tropical areas. Palaeontol. Electron. 6, 1–29.

Juggins, S., 2012. Rioja: analysis of Quaternary science data. R package version 0.8-3. Retrieved from http://cran.2-project.org/package=rioja.

Krishnamurti, T.N., Stefanova, L., Misra, V., 2013. Tropical Meteorology: An Introduction. Springer New York, New York, NY.

Labin, A.A., Siman-Tov, R., Rosenfeld, A., Debard, E., 1995. Occurrence and distribution of the foraminifer *Ammonia beccarii tepida* (Cushman) in water bodies, Recent and Quaternary, of the Dead Sea Rift, Israel. Mar. Micropaleontol. 26, 153–159.

Lamy, F., Hebbeln, D., Röhl, U., Wefer, G., 2001. Holocene rainfall variability in southern Chile: a marine record of latitudinal shifts of the Southern Westerlies. Earth Planet. Sci. Lett. 185, 369–382.

Lane, C.S., Horn, S.P., Mora, C.I., Orvis, K.H., 2009. Late-Holocene paleoenvironmental change at mid-elevation on the Caribbean slope of the Cordillera Central, Dominican Republic: a multi-site, multi-proxy analysis. Quat. Sci. Rev. 28, 2239–2260.

Lane, C.S., Horn, S.P., Orvis, K.H., Thomason, J.M., 2011. Oxygen isotope evidence of Little Ice Age aridity on the Caribbean slope of the Cordillera Central, Dominican Republic. Quat. Res. 75, 461–470.

Lane, C.S., Clark, J.J., Knudsen, A., McFarlin, J., 2013. Late-Holocene paleoenvironmental history of bioluminescent Laguna Grande, Puerto Rico. Palaeogeogr. Palaeoclimatol. Palaeoecol. 369, 99–113.

Lane, C.S., Horn, S.P., Kerr, M.T., 2014. Beyond the Mayan Lowlands: impacts of the Terminal Classic Drought in the Caribbean Antilles. Quat. Sci. Rev. 86, 89–98.

Löwemark, L., Chen, H.F., Yang, T.N., Kylander, M., Yu, E.F., Hsu, Y.W., Lee, T.Q., Song, S.R., Jarvis, S., 2011. Normalizing XRF-scanner data: a cautionary note on the interpretation of high resolution records from organic-rich lakes. J. Asian Earth Sci. 40, 1250–1256.

Mahiques, M.M., Wainer, I.K.C., Burone, L., Nagai, R., Sousa, S.H., Figueira, R.C.L., Silveira, I.C.A., Bicego, M.C., Alves, D.P.V., Hammer, O., 2009. A high-resolution Holocene record on the Southern Brazilian shelf: paleoenvironmental implications. Quat. Int. 206, 52–61.

Malaizé, B., Bertran, P., Carbonel, P., Bonnissent, D., Charlier, K., Galop, D., Imbert, D., Serrand, N., Stouvenot, C., Pujol, C., 2011. Hurricanes and climate in the Caribbean during the past 3700 years BP. The Holocene 21, 911–924.

Masson-Delmotte, V., Kageyama, M., Braconnot, P., Charbit, S., Krinner, G., Ritz, C., Guilyardi, E., Jouzel, J., Abe-Ouchi, A., Crucifix, M., Gladstone, R.M., Hewitt, C.D., Kitoh, A., LeGrande, A.N., Marti, O., Merkel, U., Motoi, T., Ohgaito, R., Otto-Bliesner, B., Peltier, W.R., Ross, I., Valdes, P.J., Vettoretti, G., Wber, S.L., Wolk, F., Yu, Y., 2005. Past and future polar amplification of climate change: climate model intercomparisons and ice-core constraints. Clim. Dyn. 26, 513–529.

McCloskey, T.A., Keller, G., 2009. 5000 year sedimentary record of hurricane strikes on the central coast of Belize. Quat. Int. 195, 53–68.

Medina-Elizalde, M., Burns, S.J., Lea, D.W., Asmerom, Y., Gunten, L.V., Polyal, V., Vuille, M., Karmalkar, A., 2010. High resolution stalagmite climate record from the Yucatán Peninsula spanning the Maya terminal classic period. Earth Planet. Sci. Lett. 298, 255–262.

Milne, G., Peros, M.C., 2013. Data-model comparison of Holocene sea-level change in the circum-Caribbean region. Glob. Planet. Chang. 107, 119–131.

Mora, G., Martinez, J., 2005. Sedimentary metal ratios in the Colombia Basin as indicators for water balance change in northern South America during the past 400,000 years. Paleoceanography 20 PA4013.

Moy, C.M., Seltzer, G.O., Rodbell, D.T., Anderson, D.M., 2002. Variability of El Niño/Southern Oscillation activity at millennial timescales during the Holocene epoch. Nature 420, 162–165.

Murray, J.W., 1991. Ecology and Palaeoecology of Benthic Foraminifera. Longman Scientific and Technical, Harlow, Essex, England: New York.

Oliva, G., Instituto Geográfico Nacional (Spain), 1989. Instituto de Geografía (Academia de Ciencias de Cuba). 1a edición Instituto de Geografía de la Academia de Ciencias de Cuba, Havana.

Patterson, T., Fishbein, A., 1989. Re-examination of the statistical methods used to determine the number of point counts needed for micropaleontological quantitative research. J. Paleontol. 63, 245–248.

Peros, M.C., Reinhardt, E.G., Schwarcz, H.P., Davis, A.M., 2007a. High-resolution paleosalinity reconstruction from Laguna de la Leche, north coastal Cuba, using Sr, O, and C isotopes. Palaeogeogr. Palaeoclimatol. Palaeoecol. 245, 535–550.

Peros, M.C., Reinhardt, E.G., Davis, A.M., 2007b. A 6000-year record of ecological and Hydrological changes from Laguna de la Leche, north coastal Cuba. Quat. Res. 67, 69–82.

Pilarczyk, J.E., Reinhardt, E.G., 2012. *Homotrema rubrum* (Lamarck) taphonomy as an overwash indicator in marine ponds on Anegada, British Virgin Islands. Nat. Hazards 63, 85–100.

Poag, C.W., 1981. Ecologic Atlas of Benthic Foraminifera, of the Gulf of Mexico. Hutchinson Ross Publishing Company, Massachusetts, United States.

Reimer, P.J., Bard, E., Bayliss, A., Beck, J.W., Blackwell, P.G., Bronk Rmasey, C., Buck, C.E., Edwards, R.L., Friedrich, M., Grootes, P.M., Guilderson, T.P., Haflidason, H., Hajdas, I., Hatté, C., Heaton, T.J., Hoffman, D.L., Hogg, A.G., Hughen, K.A., Kaiser, K.F., Kromer, B., Manning, S.W., Niu, M., Reimer, R.W., Richards, D.A., Scott, D.E.M., Southon, J.R., Turney, C.S.M., van der Plicht, J., 2013. IntCal13 and Marine13 radiocarbon age calibration curves, 0–50,000 years cal BP. Radiocarbon 55, 1869–1887.

Rothwell, R.G., 2006. New Techniques in Sediment Core Analysis. Geological Society of London Special Publications, London.

Rothwell, G.R., Hoogakker, B., Thomson, J., Croudace, I.W., Frenz, M., 2006. Turbidite emplacement on the southern Balearic Abyssal Plain (western Mediterranean Sea) during Marine Isotope Stages 1–3: an application of ITRAX XRF scanning of sediment cores to lithostratigraphic analysis. In: Rothwell, R.G. (Ed.), New Techniques in Sediment Core Analysis. Geological Society of London Special Publications, London, pp. 79–89.

Sáez, A., Valero-Garcés, B.L., Giralt, S., Moreno, A., Bao, R., Pueyo, J.J., Hernández, A., Casas, D., 2009. Quat. Sci. Rev. 28, 2743–2759.

Seifriz, W., 1943. The plant life of Cuba. Ecol. Monogr. 13, 375–426.

Shotton, F.W., 1972. An example of hard-water error in radiocarbon dating vegetable matter. Nature 240, 460–461.

Simpson, G.L., Oksanen, J., 2013. Analogue: analogue matching and modern analogue technique transfer function models. R package version 0.12-0. Retrieved from http://cran.r-project.org/package=analogue.

Sloan, L.C., Barron, E.J., 1992. A comparison of Eocene climate model results to quantified paleoclimatic interpretations. Palaeogeogr. Palaeoclimatol. Palaeoecol. 93, 183–202.

Smith, S.M., Snedaker, S.C., 1995. Salinity responses in two populations of viviparous *Rhizophora mangle* L. seedlings. Biotropica 27 (4), 435–440.

Thanachit, S., Suddhiprakarn, A., Kheorueromne, I., Gikes, R.J., 2006. The geochemistry of soils on a catena on basalt at Khon Buri, northeast Thailand. Geoderma 135, 81–96.

Thomson, J., Croudace, I.W., Rothwell, R.G., Rothwell, R.G., 2006. A geochemical application of the ITRAX scanner to a sediment core containing eastern Mediterranean sapropel units. New Techniques in Sediment Core Analysis. Geological Society of London Special Publications, London, pp. 65–77.

Toscano, M.A., Macintyre, I.G., 2003. Corrected western Atlantic sea-level curve for the last 11,000 years based on calibrated 14C dates from Acropora palmata framework and intertidal mangrove peat. Coral Reefs 22, 257–270.

Van Hengstum, P.J., Reinhardt, E.G., Beddows, P.A., Gabriel, J.J., 2010. Linkages between Holocene paleoclimate and paleohydrogeology preserved in a Yucatan underwater cave. Quat. Sci. Rev. 29, 2788–2798.

Walton, W.R., Sloan, B.J., 1990. The Genus *Ammonia* Brunnich, 1772: its geographic distribution and morphologic variability. J. Foraminifer. Res. 20, 128–156.

Wang, C., Enfield, D.B., Lee, S.-K., Landsea, C.W., 2006. Influences of the Atlantic Warm Pool on western hemisphere summer rainfall and Atlantic hurricanes. J. Clim. 19, 3011–3028.

Warrier, A.K., Shankar, R., 2009. Geochemical evidence for the use of magnetic susceptibility as a paleorainfall proxy in the tropics. Chem. Geol. 265, 553–562.

Weltje, G.J., Tjallingii, R., 2008. Calibration of XRF core scanners for quantitative geochemical logging of sediment cores: theory and application. Earth Planet. Sci. Lett. 274 (3–4), 423–438.

Woodruff, J.D., Donnelly, J.P., Mahrig, D., Geyer, W.R., 2008. Reconstructing relative flooding intensities responsible for hurricane-induced deposits from Laguna Playa Grand, Vieques, Puerto Rico. Geology 36, 391–394.

Wooller, M.J., Behling, H., Guerrero, J.L., Jantz, N., Zweigert, M.E., 2009. Late Holocene hydrologic and vegetation changes at Turneffe Atoll, Belize, compared with records from mainland Central America and Mexico. PALAIOS 24, 650–656.

Wurtzel, J.B., Black, D.E., Thunnell, R.C., Peterson, L.C., Tappa, E.J., Rahman, S., 2013. Mechanisms of southern Caribbean SST variability over the last two millennia. Geophys. Res. Lett. 40, 5954–5958.

Yao, Z., Liu, Y., Shi, X., Suk, B.C., 2012. Paleoenvironmental changes in the East/Japan Sea during the last 48 ka: indications from high-resolution X-ray fluorescence core scanning. J. Quat. Sci. 28, 932–940.

Yarincik, K., Murrary, R., Peterson, L.C., 2000. Climatically sensitive eolian and hemipelagic deposition in the Cariaco Basin, Venezuela, over the past 578,000 years: Results from Al/Ti and K/Al. Paleoceanography 15, 210–228.

Zabel, M., Schneider, R.R., Wagner, T., Adegbie, A.T., Vreis, U., Kolonic, S., 2001. Late Quaternary climate changes in Central Africa, as inferred from terrigenous input to the Niger Fan. Quat. Res. 56, 207–217.